Spin-density-wave transition of Fe1 zigzag chains and metamagnetic transition of Fe2 in $TaFe_{1+y}Te_3$

R. H. Liu, M. Zhang, P. Cheng, Y. J. Yan, Z. J. Xiang, J. J. Ying, X. F. Wang, A. F. Wang, G. J. Ye, X. G. Luo, and X. H. Chen*

Hefei National Laboratory for Physical Science at Microscale and Department of Physics, University of Science and Technology of China, Hefei, Anhui 230026, People's Republic of China

(Received 13 July 2011; published 28 November 2011)

The mixed-metal-network layered compound $TaFe_{1+x}Te_3$ has the $TaFeTe_3$ layers formed by Ta-Fe bonded network (Fe1) sandwiched with tellurium layers and the excess iron atoms (Fe2) partially occupying the interstitial site of the tetrahedral (Ta,Fe)Te at random, which are similar to the interstitial iron atoms in the iron-based high-T_c superconductor $Fe_{1+y}Te$. The antiferromagnetic (AFM) transition of Fe1 zigzag chains and spin flop of these interstitial Fe2 atoms under a high magnetic field are studied through susceptibility, magnetoresistance (MR), the Hall effect, and specific heat measurements in high-quality single-crystal $TaFe_{1+y}Te_3$. These properties suggest that the high-temperature AFM transition of the $TaFeTe_3$ layers should be a spin-density-wave-type AFM order. Below T_N, the spin flop of these interstitial Fe2 from antiferromagnetism to ferromagnetism induces a sharp drop on resistivity and an anomalous Hall effect. It can be inferred from the spin flop of Fe2 that the local moment of Fe2 atom is about 4 μ_B/Fe. The possible magnetic structure of $TaFe_{1+y}Te_3$ is proposed from the susceptibility, MR, and Hall effect. The properties related to the spin flop of Fe2 supply a good opportunity to study the coupling between Fe1 and Fe2 in these $TaFe_{1+y}Te_3$ or $Fe_{1+y}Te$ compounds with interstitial Fe2.

DOI: 10.1103/PhysRevB.84.184432 PACS number(s): 75.50.Ee, 75.30.Gw, 75.30.Kz, 74.70.Xa

I. INTRODUCTION

The discovery of iron-based high-temperature superconductors has generated great interest in exploring layered Fe-based pnictides and chalcogenides.[1–4] The superconducting transition temperature (T_c) in iron chalcogenides α-FeSe increased from 8 K[4] to 15 K by partial Te substitution for Se[5,6] and up to 37 K under high pressure.[7,8] Recently, the new intercalated iron selenides $A_xFe_{2-y}Se_2$ (A = K, Rb, Cs, and Tl)[9–12] were reported to have T_c around 32 K and even 43 K. Although the presently known maximum critical temperatures are lower than that of iron pnictides, iron chalcogenides have attracted considerable attention because they are virulent As free and have very interesting coexistence and competition relationships between magnetism and superconductivity.[13,14] The observation of spin resonance below T_c and enhancement of spin fluctuation near T_c in iron chalcogenides suggests a superconducting pairing mechanism mediated by spin fluctuation. The high-pressure and muon-spin-rotation (μSR) experiments indicate the static magnetic phase microscopically coexists with superconductivity in $FeSe_{1-x}$ under pressure. In addition, the magnetic order temperature (T_N) and superconducting transition temperature (T_c) are both enhanced by pressure.[13,14] In the intercalated iron selenides, μSR,[15,16] neutron scattering,[17] and high-temperature magnetization and resistivity[18] also indicate that superconductivity coexists with antiferromagnetism (AFM) with high T_N (T_N = 470–550 K) and large magnetic moment 2–3.3 μ_B/Fe.[16,17] Furthermore, $Fe_{1+y}Te$ has the most simple crystal structure in iron-based superconductors. It is stacked with anti-PbO-type FeTe layer along the c axis, in which iron atoms (Fe1) form a square plane in the edge-sharing FeTe tetrahedral layer. $Fe_{1+y}Te$ always contains excess iron atoms (Fe2), which randomly occupy the interstitial sites of the FeTe layer and directly couple with the four nearest-neighbor Fe1 atoms in the iron square plane.[19,20] This structural characteristic is analogous to that of PbFCl-type Fe_2As, where half of the iron atoms (Fe1) and As form an edge-sharing tetrahedral network and the other half of the iron atoms (Fe2) fully occupy these interstitial sites between anti-PbO-type FeAs layers. The Fe_2As compound also has a spin-density-wave (SDW)–type AFM order at 353 K,[21] which is higher than T_N in FeAs-based parent compounds.

$Fe_{1+y}Te$ is not superconducting until Te atoms are partially replaced by Se or S and excess iron atoms (Fe2) are also removed simultaneously.[5,6] Similar to iron pnictides, $Fe_{1+y}Te$ exhibits a structural and AFM transition simultaneously near $T_N \sim$ 60–70 K. The different T_N arise from the different contents of excess partial iron atoms (Fe2).[4–6,19,20] However, its AFM structure is distinct from that in FeAs-based parent compounds. A collinear commensurate AFM order with Fe moment along the a axis has been identified in the iron-pnictides,[22,23] while $Fe_{1+y}Te$ has a bicollinear and 45° rotated AFM order.[24,25] In addition, a neutron-scattering experiment found that interstitial Fe2 could tune the AFM wave vector from commensurate to incommensurate in $Fe_{1+y}Te$ when y is increased to above 0.076. Theory suggests that the interstitial Fe2 with a valence near Fe^+ donates charge to the FeTe layers.[26] There is also a very strong tendency toward moment formation on Fe2, and then these interstitial Fe2 with a large local moment will interact with the magnetism of the FeTe layers, complicating the magnetic order.[24–27] Here we report a mixed-metal-network layered compound $TaFe_{1+y}Te_3$, which consists of the "sandwich" $TaFeTe_3$ layers (Fe1) and the excess iron atoms (Fe2) partially occupying the interstitial site of the tetrahedral (Ta,Fe)Te at random,[28–30] similar to those in $Fe_{1+y}Te$. $TaFe_{1+y}Te_3$ has a SDW-type AFM order (T_N) at 160–200 K, depending on the contents of interstitial Fe2 atoms. In addition, below T_N, these Fe2 atoms directly couple with the three nearest Fe1 atoms of Ta-Fe1 mixed network layers and form an AFM alignment. However, an external magnetic field ($\mathbf{H}_{ext}$) is able to break the coupling between Fe1 and Fe2, causing Fe2 to take a spin flop and form ferromagnetic (FM) alignment from AFM alignment. It offers an interesting opportunity to investigate the interplay between excess Fe2 and

magnetism and transport properties of a Ta-Fe mixed-network layer.

II. EXPERIMENTAL DETAILS

Single crystals of $TaFe_{1+y}Te_3$ were grown by the chemical vapor transport method.[28,29] Ta (3N) powder, Fe (3N) powder, and Te (4N) powder were accurately weighed according to the stoichiometric ratio of $TaFe_{1+y}Te_3$ ($y = 0$–0.25), thoroughly ground, and pressed into pellets. The 2-g pellets and 30 mg of transport agent $TeCl_4$ were sealed in evacuated quartz tubes 18 cm long × 15 mm in diameter. The sealed tubes were placed in a multizone tube furnace and slowly heated to temperature with the hot end at 690 °C and the cool end at 630 °C. After 150 h, the furnace was shut off and cooled to room temperature. Long, narrow crystals were obtained, but in different temperature zones the samples had different contents of interstitial Fe2. Except for annealing, the sample-preparation process was carried out in a glove box in highly pure argon atmosphere. Single-crystal x-ray diffraction (XRD) was performed on a MAC MXPAHF x-ray diffractometer (Japan) at room temperature. Elemental analysis was obtained by energy-dispersive x-ray spectroscopy (EDX). Magnetic susceptibility measurements were performed on a Squid magnetometer (Quantum Design MPMS-XL7s). Magnetoresistance (MR), Hall coefficient (R_H), heat capacity, and thermoelectric power (TEP) were measured on a Quantum Design PPMS.

III. RESULTS AND DISCUSSION

A. Crystal structure

The structure of $TaFe_{1+y}Te_3$ is shown in the right inset of Fig. 1(a). The structure of $TaFe_{1+y}Te_3$ features a Ta-Fe bonded network, and the mixed-metal network lies between tellurium layers, forming a $FeTaTe_3$ "sandwich,"[28,29,31] similar to that of anti-PbO-type FeTe layer. It is stacked with a $FeTaTe_3$ sandwich along $(-l\ 0\ l)$ and crystallizes in $P2_1/m$ monoclinic symmetry with lattice constants $a = 7.4262$ Å, $b = 3.6374$ Å, $c = 9.9925$ Å, and $\beta = 109.166°$. According to the literature,[28,30] there are always partial excess iron atoms, which randomly occupy the interstitial sites of $FeTaTe_3$ layers,[30] similar to those in $Fe_{1+y}Te$. Figure 1(a) shows an XRD pattern of the platelet-shaped $TaFe_{1+y}Te_3$ single crystal at room temperature. Only $(-l\ 0\ l)$ reflections are observed in the XRD pattern, indicating that the $FeTaTe_3$ sandwich plane parallels to the surface of the long piece-like single crystal. The full width at half maximum (FWHM) in the rocking curve of the (−3 0 3) reflection is 0.1°, as shown in the left inset of Fig. 1(a), which suggests it is a high-quality single crystal. A view of the $FeTaTe_3$ sandwich structure along the b axis is shown in Fig. 1(b). There are two unique zigzag chains that are parallel to the b axis. The view nearly perpendicular to the Ta-Fe mixed network layer is shown in Fig. 1(c). One can easily see that one chain consists of Ta-centered octahedra, which share Te-Ta edges. The other chain is made up of Fe-centered edge-sharing tetrahedra. These two zigzag chains alternately build up the Ta-Fe mixed networks. From another point of view, the Ta-Fe mixed-metal $FeTaTe_3$ layer is made up of (Ta,Fe)Te tetrahedra Ta-Fe-Fe-Ta ribbons contacted by sharing-edge Te-Te. The coordination environment of Fe1 in the $FeTaTe_3$ sandwich layer is the same as that of $FeTe_4$ tetrahedra in the anti-PbO-type FeTe layer. Additionally, there are excess partial Fe2 atoms randomly occupying square pyramidal sites formed by five Te atoms. The $(Ta,Fe)Te_4$ tetrahedra structure of the $FeTaTe_3$ sandwich layer and the $Fe_{1+y}Te$ structure are shown in Figs. 1(d) and 1(e), respectively.

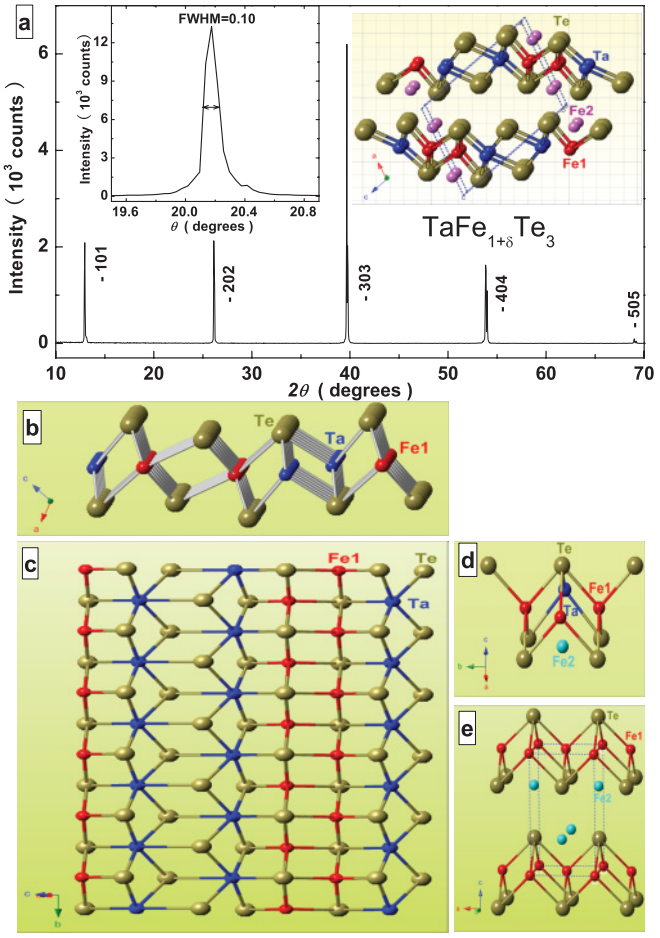

FIG. 1. (Color online) (a) The single-crystal x-ray diffraction pattern for $TaFe_{1+y}Te_3$. The left inset shows the rocking curve at the (−3 0 3) reflection. The crystal structure is shown in the right inset. (b) A view of the $TaFeTe_3$ "sandwiched" structure along the b axis. There are two unique zigzag chains that are parallel to the b axis. (c) A view of the mixed-metal-network $TaFeTe_3$ along $(-l\ 0\ l)$; (d) The zigzag chain is made up of Fe centered edge-sharing tetrahedra, similar to the $FeTe_4$ tetrahedra of anti-PbO-type $Fe_{1+y}Te$. The partial Fe2 atoms randomly occupy the interstitial sites of the (Ta,Fe)Te layers. (e) The structure of anti-PbO-type $Fe_{1+y}Te$. The partial Fe2 atoms also randomly occupy the interstitial sites of anti-PbO-type FeTe layers.

B. Magnetic susceptibility and magnetoresistance

Temperature dependence of susceptibility under different magnetic fields perpendicular and parallel to the plane of the single crystal are shown in Figs. 2(a) and 2(b), respectively. From the single-crystal XRD pattern, we know that the Ta-Fe mixed-metal network is parallel to the plane of the single crystal. The susceptibility under low field shows a sharp antiferromagnetic transition at $T_N \sim 160$ K, which is lower

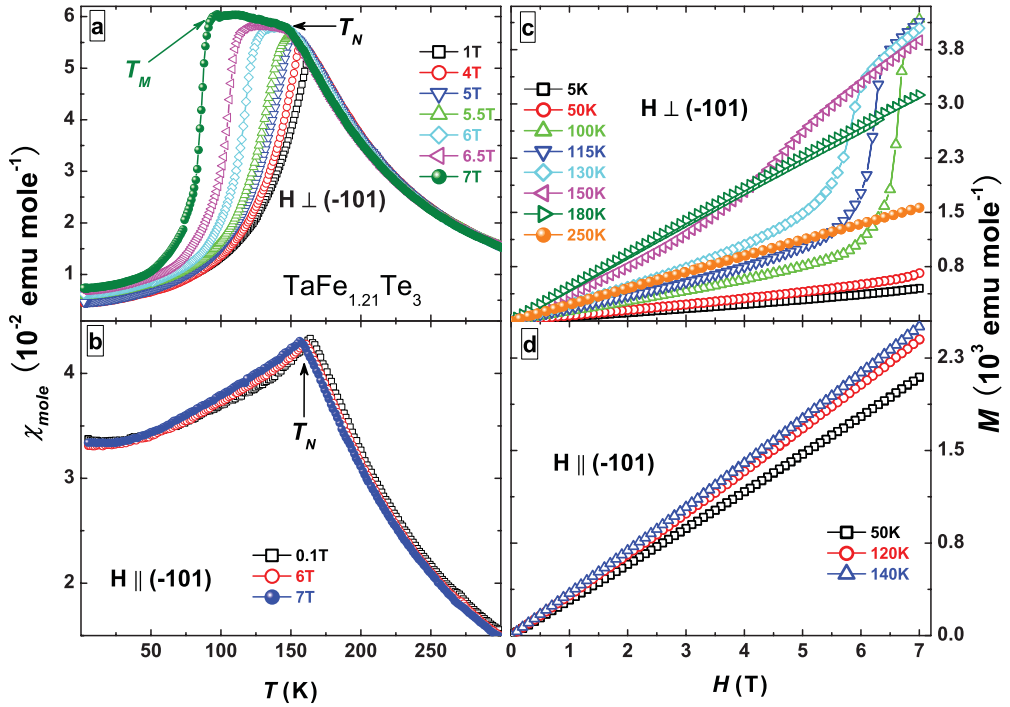

FIG. 2. (Color online) Temperature dependence of susceptibility measured under different fields perpendicular to sample plane (a) or along sample plane (b). Field dependence of magnetization **M** at various temperature with field perpendicular to sample plane (c) or along sample plane (d).

than the $T_N = 200$ K transition of polycrystalline sample $TaFe_{1.25}Te_3$.[28] Elemental analysis of the single crystal with $T_N = 160$ K obtained by EDX indicates that interstitial iron is about 0.21. This suggests that interstitial iron atoms Fe2 have strong effects on the magnetism of the Fe zigzag chains. Less excess iron will result in lower T_N. When an external magnetic field is perpendicular to the Ta-Fe mixed-metal network, the AFM order temperature T_N is weakly suppressed from $T_N = 160$ K at 0.1 T to $T_N = 150$ K at 7 T, and the more interesting thing is that in the high magnetic field the susceptibility exhibits ferromagnetic behavior below T_N. Below T_N, susceptibility first is constant with decreasing temperature and then sharply drops at a certain temperature T_M, which depends on the magnitude of external field **H**. At 160 K, Fe1 atoms of zigzag chains form an AFM order and also induce excess Fe2 atoms of interstitial sites to form an AFM order simultaneously due to the direct coupling of Fe1 and Fe2. Below T_N, the magnetic moment of excess Fe2 tends to align along the direction of external field H and forms a ferromagnetic order due to the coupling of Fe2 and the external field. This is the reason why susceptibility is constant under a higher vertical magnetic field below T_N. The external field $\mathbf{H}_{\text{ext}}$ and the inner field $\mathbf{H}_{\text{int}}$ formed by Fe1 zigzag chains compete in tuning direction of magnetic moment of Fe2 below T_N. The external field is in the ascendant in tuning Fe2 to form a FM alignment at high temperature, while the inner field will be in the ascendant with decreasing temperature, which also induces the susceptibility to drop sharply at a certain temperature. The susceptibility of a single crystal has strong anisotropic magnetic properties at low field below T_N, suggesting that the magnetic easy axis of Fe1 zigzag is along the $[-l\ 0\ l]$. Figures 2(c) and 2(d) show the field dependence of magnetization **M** at various temperatures with fields perpendicular and parallel to the Ta-Fe mixed network, respectively. When the external magnetic field is perpendicular to Fe1 zigzag of the Ta-Fe mixed network, magnetization **M** increases linearly with the external field $\mathbf{H}_{\text{ext}}$ at low field and shows a sharp ferromagnetic-like transition at certain field H_C. However, the magnetic hysteresis is not observed in M-H curves at Figs. 2(c) and 2(d). It also arises from the external field $\mathbf{H}_{\text{ext}}$ competing with the inner field $\mathbf{H}_{\text{int}}$ formed by Fe1 zigzag chains for tuning the direction of Fe2 spin.

Figure 3 shows the temperature dependence of resistivity in various magnetic fields **H**. The resistivity shows the metal behavior and has an abnormal transition at $T_{S1} \sim 160$ K under low field, corresponding to the drop of magnetic susceptibility. When external magnetic field is parallel to the Ta-Fe mixed-metal network, the abnormal transition temperature T_{S1} has almost no change at different fields. However, under a high field perpendicular to the single-crystal plane, T_{S1} is weakly suppressed to low temperature ($T_{S1} = 150$ K for $\mathbf{H} > 6$ T) and the resistivity has another abnormal transition simultaneously at a certain low temperature T_{S2}, which depends on the magnitude of external field **H**. These abnormal behaviors of resistivity can be easily seen in these insets of Fig. 3. The T_{S1} and T_{S2} in resistivity correspond to the AFM transition temperature T_N of Fe1 and the metamagnetic transition temperature T_M of Fe2 in magnetic susceptibility, respectively.

To confirm the origin of the anomalous resistivity, isothermal MR at different temperatures is shown in Fig. 4. One can easily see the negative MR effect under a parallel field for all temperatures and under a vertical field for temperatures higher

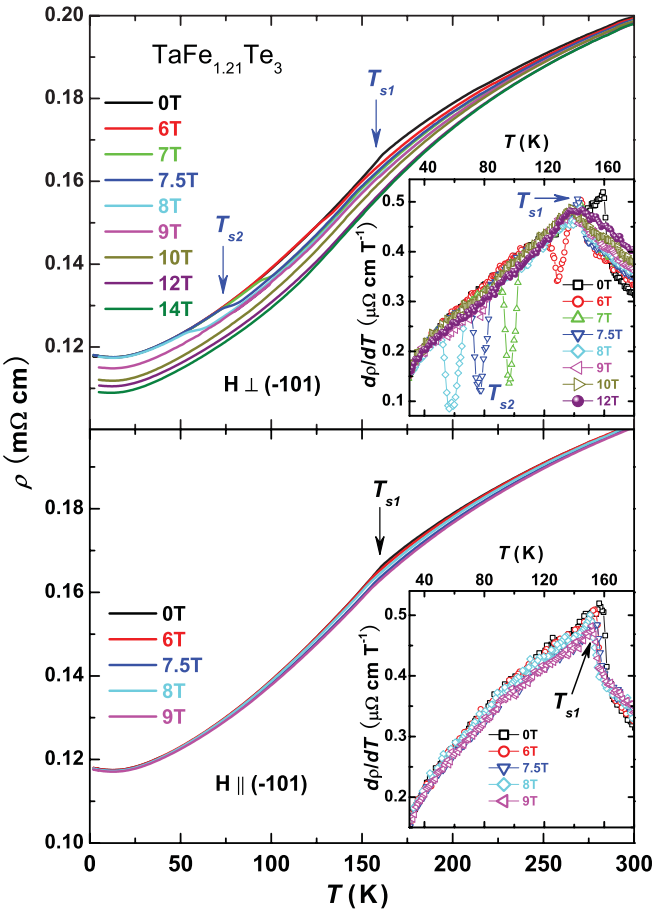

FIG. 3. (Color online) Temperature dependence of resistivity under different fields perpendicular to the sample plane (top panel) or along the sample plane (bottom panel). Inset: Temperature dependence of their derivative resistivities $d\rho/dT$.

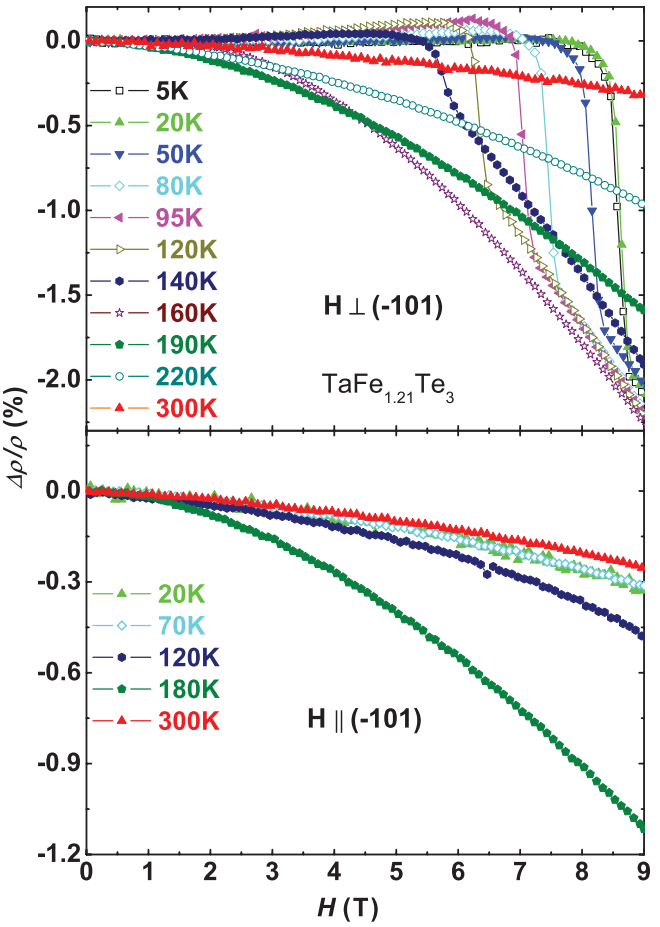

FIG. 4. (Color online) Isothermal magnetoresistance at different temperatures with field perpendicular to the sample plane (top panel) or along the sample plane (bottom panel).

than T_N. For a vertical field, small positive MR is observed below the certain field H_C, and a sharp negative MR is shown around H_C, which should be ascribed to the spin flop of Fe2 at a certain field H_C. The largest negative MR effect, appearing at a temperature slightly higher than T_N, suggests that there is a strong magnetic fluctuation around T_N. The temperature dependence of a normal Hall coefficient R_H also supports this point of view.

Figure 5 shows the "spontaneous" magnetization **M** of Fe2, which is inferred from the jump magnitudes ΔM in the isothermal magnetization. The saturation magnetization at 5 K is $4 \pm 0.2\ \mu_B$ per Fe2, which is the same with local moment Fe ($4\ \mu_B$/Fe) in $Fe_{1/4}TaS_2$. The transition-metal intercalated dichalcogenide $Fe_{1/4}TaS_2$ has a ferromagnetic transition at $T_C \sim 160$ K, in which the spontaneous magnetization of Fe is strongly pinned perpendicular to the TaS_2 layers by a very large anisotropy field below T_C.[32] Neutron scattering experiments reveal that the Fe has a total moment of 2.25(8) μ_B/Fe in $Fe_{1+y}Te$.[25] Since the moments of the partial Fe2 ions are randomly distributed in the interstitial sites of FeTe layers, it is difficult to estimate the moment sizes of excess Fe2 by using conventional neutron diffraction.[24,25] However, the theoretical calculation suggests that the excess Fe2 has very strong magnetism with high local moment.[26] We find that magnetization of excess Fe2 has a near-perfect T^2 dependence below T_N, which is in agreement with normal ferromagnetic metals,[33] as shown in Fig. 5. The spin flop of Fe2 tuned by a field induces a sharp negative MR $[\Delta\rho(T)/\rho(T)]$ around H_C, as shown in Fig. 5. $\Delta\rho(T)/\rho(T)$ and magnetization **M** of Fe2 have the same dependence of temperature. $\frac{\Delta\rho/\rho}{M_{Fe2}}$ is about 0.45% per μ_B (Fe2). We use the Curie-Weiss expression $\chi = \chi_o + C/(T + \Theta)$ to fit the susceptibility data from 330 to 400 K, where C is the Curie constant, Θ is the Weiss temperature, and χ_o is constant. The total effective moment of 3.9 μ_B per iron atom is obtained from the Curie constant. It is a little larger than the result of 3.7 μ_B given in previous literature reports, in which the susceptibility of the polycrystalline sample is fitted by the Curie-Weiss expression from 450 to 1000 K.[28] From MR and the following Hall coefficient result, we know that there is very strong magnetic fluctuation or magnetic correlation between iron atoms above T_N. The temperature range of susceptibility fitted from 330 to 400 K is too low and brings some deviation of inferred total effective moment. In spite of the small deviation, the magnetic moment of the Fe1 ($3.7 \pm 0.2\ \mu_B$) in Ta-Fe-Fe-Ta ribbons of the $TaFeTe_3$ sandwich is almost two times larger than that of Fe1 (2.25 μ_B) in the anti-PbO-type FeTe layers.

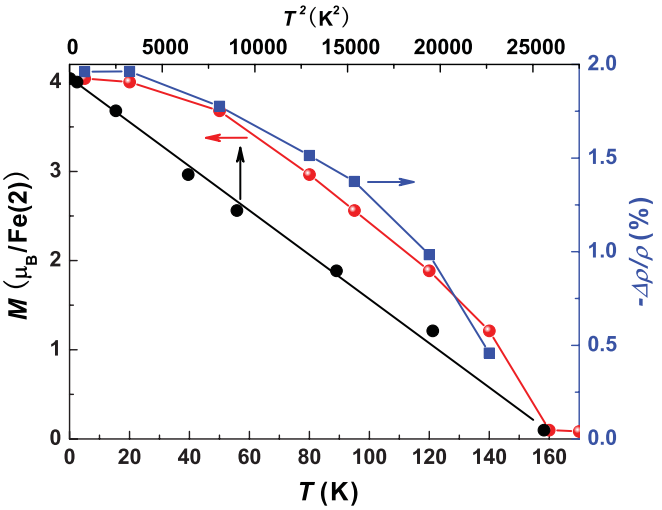

FIG. 5. (Color online) Magnetization of Fe2 **M** vs T (left y axis) and magnetoresistance $\Delta\rho(T)/\rho(T)$ vs T (right y axis). $\boldsymbol{M}$ vs T^2 (top x axis) shows $\Delta M(T)/M(0) \propto T^2$ up to 160 K.

C. Hall coefficient and thermoelectric powder

It is well known that the Hall effect arises from two parts of normal Hall effect and anomalous Hall effect in ferromagnetic metals, in which anomalous Hall resistivity is proportional to the magnetization **M**. Empirically, one finds Hall resistivity $\rho_H = \rho_{OH} + \rho_{AH} = R_H^N + R_H^A 4\pi M$, where ρ_{OH} is the normal Hall resistivity due to the Lorentz force in a perpendicular magnetic field **B**, ρ_{AH} is the anomalous Hall resistivity, R_H^N is the normal Hall coefficient, and R_H^A is the anomalous Hall coefficient.[34] To confirm the origin of the AFM transition of Fe1 zigzag chains and field-inducing FM transition of Fe2, the transverse resistivity ρ_{xy} is measured by sweeping the field from −9 T to +9 T at various temperatures, and the accurate Hall resistivity ρ_H is obtained, as shown in Fig. 6(a), by using $[\rho_{xy}(+H) - \rho_{xy}(-H)]/2$, where $\rho_{xy}(\pm H)$ is ρ_{xy} under a positive or negative magnetic field. Similar to the isothermal MR at various temperature, ρ_H also shows a steep rise at a certain field H_C below T_N, which arises from the jump magnitudes of magnetization **M** due to the spin flop of excess Fe2 induced by external field **H**. The normal Hall coefficient R_H^N is obtained from the H-linear term of ρ_H below the "coercive" field H_C. R_H^N dependence of temperature is shown in Fig. 5. The R_H^N is positive, indicating the carrier is hole-type. Above T_N, R_H^N decreases distinctly with increasing temperature and has an almost linear dependence on temperature. It may arise from the strong magnetic fluctuation above T_N in this system. Empirically, the change of R_H^N is weakly dependent on temperature above T_C in general ferromagnetic metal. R_H^N shows a pronounced dip at T_N because the magnetic fluctuation is suppressed completely and the transport lifetime τ has a strong change around the fermi surface below T_N. The Hall number density $n_H = 1/eR_H^N$ varies from the minimal value 1.3×10^{21} cm^{-3} at 155 K to 1.4×10^{22} cm^{-3} at 75 K. The normal Hall coefficient R_H^N is the same order of magnitude as that of $Fe_{1+y}Te$ ($R_H \sim 10^{-9}$m^3/C).[27] The TEP is positive and has the same sign as the Hall coefficient. As shown in Fig. 6(b), TEP shows a weak temperature dependence above $T_N \sim$ 160 K, but it has a pronounced rise below

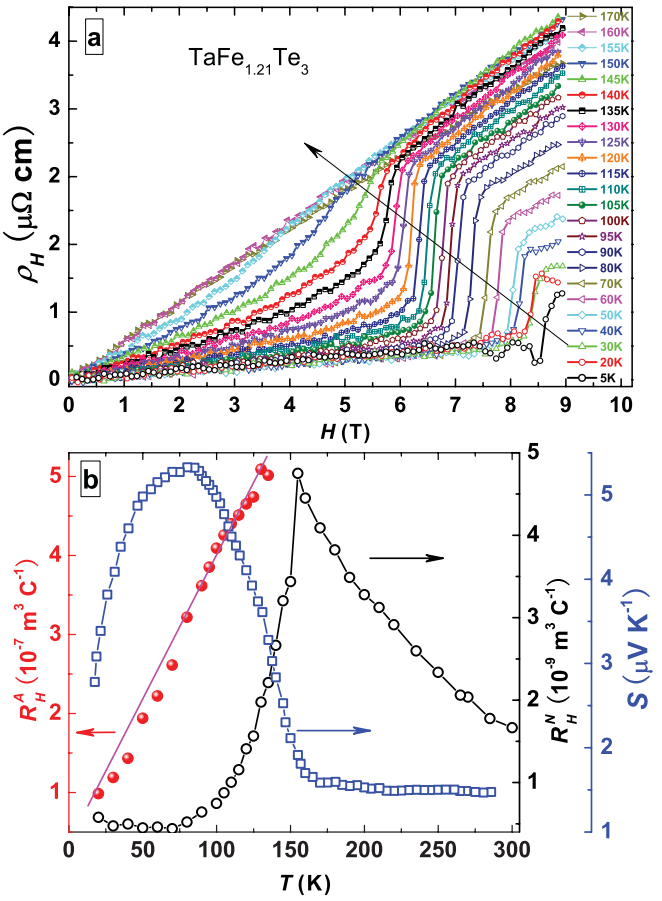

FIG. 6. (Color online) (a) Field-dependent Hall resistivities ρ_H at various temperatures are obtained by using $[\rho_{xy}(+H) - \rho_{xy}(-H)]/2$, where $\rho_{xy}(\pm H)$ is ρ_{xy} under positive or negative magnetic fields. (b) The temperature dependence of the anomalous Hall coefficient R_H^A, normal Hall coefficient R_H^N, and thermoelectric power S. R_H^A is inferred from the jump in ρ_H at "coercive" field H_C, while R_H^N is inferred from the H-linear portions of ρ_H below H_C.

T_N and arrives at the maximum (5.2 μV/K) around 75 K. The resistivity, susceptibility, R_H^N, and TEP show anomalous behaviors below T_N, which are very similar to that in metal Cr around the SDW-type AFM transition.[35] In addition, the structure of $TaFe_{1+y}Te_3$ features Fe1 zigzag chains along the b axis. It is well known that many low-dimensional materials have SDW and charge-density-wave (CDW) instability at low temperatures.[36,37] The behaviors of these physical properties at T_N suggest that the transition should be a SDW-type AFM transition. The anomalous Hall coefficient R_S^A below T_N is inferred from the ratio of the jump magnitudes ΔM and $\delta\rho_H$ around H_C. $R_S^A = \Delta\rho_H/4\pi M$ is also plotted in Fig. 6(b) . R_S^A decreases linearly with temperature below T_N.

D. Heat capacity

In order to confirm the AFM transition, the heat capacity was measured by a relaxation-time method with a Quantum Design PPMS. One can clearly see a pronounced anomaly peak of $C_p(T)$ at 185 K for zero field in Fig. 7. The temperature is different from the T_N inferred by susceptibility due to different samples with different magnitude of excess Fe. The sample for specific heat measurement has 0.23 interstitial Fe2 confirmed

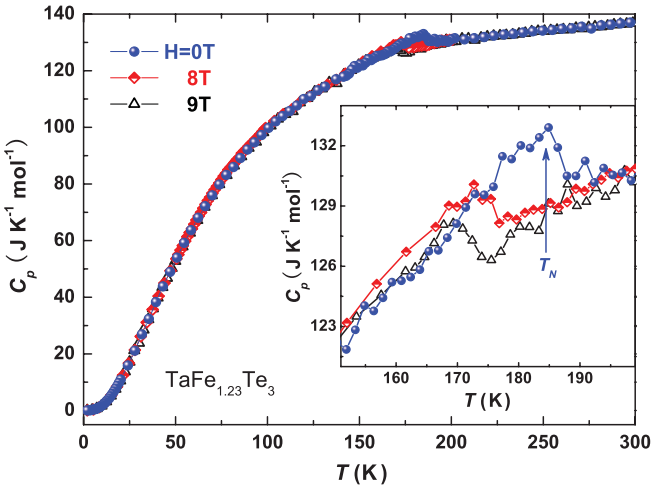

FIG. 7. (Color online) Temperature dependence of specific heat for $TaFe_{1.23}Te_3$ under different fields perpendicular to the sample plane.

by EDX. The temperature of the specific-heat peak shifts from 185 to 170 K at 9 T, which is in excellent agreement with the previous susceptibility and MR under a high magnetic field. This consistently confirms that a high magnetic field distinctly suppresses the AFM order of Fe1 zigzag chains. In the low-temperature region, the specific heat is of the form $C_p = \gamma T + \beta T^3$. The Debye temperature can be estimated from the equation $\beta = (12\pi^4 N k_B)/(5\Theta_D^3)$, where N is the number of atoms per formula unit. From the plot of C_p/T versus T^2 data between 2 and 14 K, we can estimate a Sommerfeld coefficient of $\gamma = 25.86$ mJ K^{-2} mol^{-1}, $\beta = 1.496$ mJ K^{-4} mol^{-1}, and $\Theta_D = 189$ K for $TaFe_{1.23}Te_3$. The electron specific-heat coefficient γ is close to that of $Fe_{1+y}Te$ ($\gamma = 27$ mJ K^{-2} mol^{-1}).[27] The above resistivity and normal Hall coefficient R_H^N also show that $Fe_{1+y}Te$ and $TaFe_{1+y}Te_3$ have the same order of magnitude. It suggests that $Fe_{1+y}Te$ and $TaFe_{1+y}Te_3$ have almost the same density of states near the Fermi energy level.

E. Models of magnetic structure

Based on the above results of susceptibility, MR, and Hall effect, possible magnetic structures for the spins of Fe1 and Fe2 are shown in Figs. 8(a) and 8(b). Below T_N, Fe1 atoms of zigzag chains form an antiferromagnetic alignment. The magnetic easy axis of Fe1 should be perpendicular to the Ta-Fe mixed-metal-network layers with a very large anisotropy energy. Since excess Fe2 directly couples with Fe1 of zigzag chains, the random excess Fe2 forms ferromagnetic alignment with the nearest two Fe1 due to the inner field $\mathbf{H}_{\text{int}}$ induced by Fe1 in a zigzag chain below T_N. Furthermore, the inner field and the coupling energy between Fe2 and Fe1 are both enhanced with decreasing temperature. On the other hand, the external field $\mathbf{H}_{\text{ext}}$ has very weak suppression on the AFM transition of Fe1 in zigzag chains but strongly tunes the direction of Fe2 spin as long as $\mathbf{H}_{\text{ext}} > \mathbf{H}_{\text{int}}$. Because of the crystal structure and magnetic structure shown in Fig. 8, the inner field will induce the excess Fe2 up and down among Fe1 zigzag chains to form AFM alignment between Fe2(up) and Fe2(down). That is why the whole Fe atoms form AFM alignment below T_N under a low magnetic field. However, the external field prefers the all excess Fe2 to be parallel along external field. When the external field overcomes the inner field with increasing temperature, it will tune Fe2 atoms that are antiparallel to the external field to reverse their spins. This causes susceptibility to sharply increase at a certain temperature T_M or certain field H_C, as shown in Fig. 2.

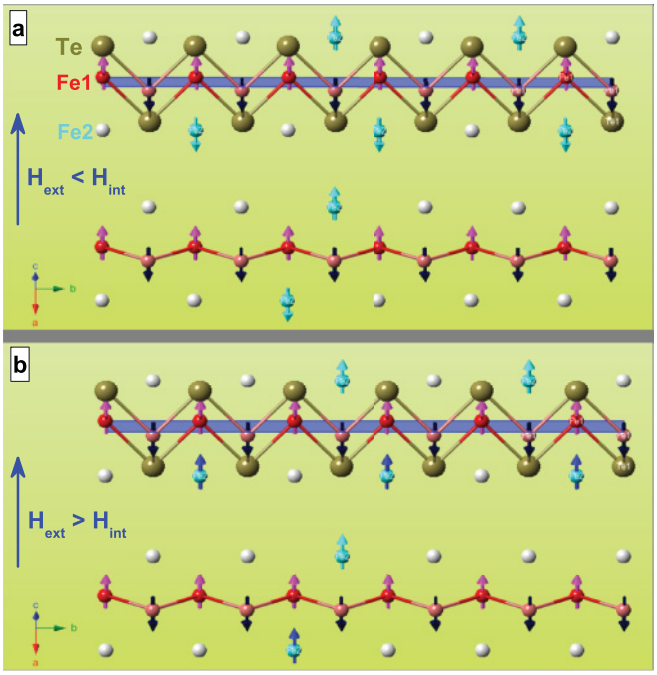

FIG. 8. (Color online) The spin model of excess Fe and Fe zigzag chain with external magnetic field $\mathbf{H}$ along $(-l\ 0\ l)$: (a) $0 \leqslant \mathbf{H}_{\text{ext}} < \mathbf{H}_{\text{int}}$; (b) $\mathbf{H}_{\text{ext}} > \mathbf{H}_{\text{int}}$.

IV. CONCLUSION

In summary, we systematically study the AFM order of Fe1 zigzag chains and spin flop of excess Fe2 under high magnetic field $\mathbf{H}$ through susceptibility, MR, Hall effect, and specific heat measurements in high-quality single-crystal $TaFe_{1+y}Te_3$. These properties suggest that the high-temperature AFM transition of the $TaFeTe_3$ layers should be a SDW-type AFM order. Below T_N, Fe1 antiferromangetic chains will induce an inner magnetic field $\mathbf{H}_{\text{int}}$ to excess Fe2 and lead Fe2 to form an AFM alignment, in which the magnetic coupling strength between Fe1 and Fe2 is enhanced by decreasing temperature. On the other hand, the external magnetic field $\mathbf{H}_{\text{ext}}$ competes with the inner magnetic field $\mathbf{H}_{\text{int}}$ induced by AFM order of Fe1 zigzag chains and inclines to tune excess Fe2 to form FM alignment along $\mathbf{H}_{\text{ext}}$. The excess Fe2 has a spin flop at the coercive field H_C, where $\mathbf{H}_{\text{ext}}$ can overcome the $\mathbf{H}_{\text{int}}$. Based on the spin flop of Fe2, the local moment of Fe2 (4 μ_B/Fe) can be obtained from $\Delta \boldsymbol{M}$ around the coercive field H_C in **M**-**H** curves. The possible magnetic structure of $TaFe_{1+y}Te_3$ is also proposed. The properties related to the spin flop of Fe2 provide a good opportunity to study the coupling between Fe1 and Fe2 in these $TaFe_{1+y}Te_3$ or $Fe_{1+y}Te$ compounds with excess Fe2.

ACKNOWLEDGMENTS

This work is supported by the National Natural Science Foundation of China (Grant No. 51021091), National Basic Research Program of China (973 Program, Grant No. 2011CB00101 and No. 2012CB922002), the Ministry of Science and Technology of China, and Chinese Academy of Sciences.

*chenxh@ustc.edu.cn

[1] Y. Kamihara, T. Watanabe, M. Hirano, and H. Hosono, J. Am. Chem. Soc. **130**, 3296 (2008).
[2] X. H. Chen, T. Wu, G. Wu, R. H. Liu, H. Chen, and D. F. Fang, Nature (London) **354**, 761 (2008).
[3] Z. A. Ren, G. C. Che, X. L. Dong, J. Yang, W. Lu, W. Yi, X. L. Shen, Z. C. Li, L. L. Sun, F. Zhou, and Z. X. Zhao, Europhys. Lett. **83**, 17002 (2008).
[4] F. C. Hsu, J. Y. Luo, K. W. Yeh, T. K. Chen, T. W. Huang, P. M. Wu, Y. C. Lee, Y. L. Huang, Y. Y. Chu, D. C. Yan, and M. K. Wu, Proc. Natl. Acad. Sci. USA **105**, 14262 (2008).
[5] K. W. Yeh, T. W. Huang, Y. L. Huang, T. K. Chen, F. C. Hsu, P. M. Wu, Y. C. Lee, Y. Y. Chu, C. L. Chen, J. Y. Luo, D. C. Yan, and M. K. Wu, Europhys. Lett. **84**, 37002 (2008).
[6] M. H. Fang, H. M. Pham, B. Qian, T. J. Liu, E. K. Vehstedt, Y. Liu, L. Spinu, and Z. Q. Mao, Phys. Rev. B **78**, 224503 (2008).
[7] Y. Mizuguchi, F. Tomioka, S. Tsuda, T. Yamaguchi, and Y. Takano, Appl. Phys. Lett. **93**, 152505 (2008).
[8] S. Medvedev, T. M. McQueen, I. A. Troyan, T. Palasyuk, M. I. Eremets, R. J. Cava, S. Naghavi, F. Casper, V. Ksenofontov, G. Wortmann, and C. Felser, Nat. Mater. **8**, 630 (2009).
[9] J. Guo, S. Jin, G. Wang, S. Wang, K. Zhu, T. Zhou, M. He, and X. Chen, Phys. Rev. B **82**, 180520 (2010).
[10] M. H. Fang, H. D. Wang, C. H. Dong, Z. J. Li, C. M. Feng, J. Chen, and H. Q. Yuan, Europhys. Lett. **94**, 27009 (2011).
[11] Y. Mizuguchi, H. Takeya, Y. Kawasaki, T. Ozaki, S. Tsuda, T. Yamaguchi, and Y. Takano, Appl. Phys. Lett. **98**, 042511 (2011).
[12] A. F. Wang, J. J. Ying, Y. J. Yan, R. H. Liu, X. G. Luo, Z. Y. Li, X. F. Wang, M. Zhang, G. J. Ye, P. Cheng, Z. J. Xiang, and X. H. Chen, Phys. Rev. B **83**, 060512(R) (2011).
[13] M. Bendele, A. Amato, K. Conder, M. Elender, H. Keller, H. H. Klauss, H. Luetkens, E. Pomjakushina, A. Raselli, and R. Khasanov, Phys. Rev. Lett. **104**, 087003 (2010).
[14] S. Margadonna, Y. Takabayashi, Y. Ohishi, Y. Mizuguchi, Y. Takano, T. Kagayama, T. Nakagawa, M. Takata, and K. Prassides, Phys. Rev. B **80**, 064506 (2009).
[15] Z. Shermadini, A. Krzton-Maziopa, M. Bendele, R. Khasanov, H. Luetkens, K. Conder, E. Pomjakushina, S. Weyeneth, V. Pomjakushin, O. Bossen, and A. Amato, Phys. Rev. Lett. **106**, 117602 (2011).
[16] V. Yu. Pomjakushin, D. V. Sheptyakov, E. V. Pomjakushina, A. Krzton-Maziopa, K. Conder, D. Chernyshov, V. Svitlyk, and Z. Shermadini, Phys. Rev. B **83**, 144410 (2011).
[17] W. Bao, Q. Huang, G. F. Chen, M. A. Green, D. M. Wang, J. B. He, X. Q. Wang, and Y. Qiu, Chin. Phys. Lett. **28**, 086104 (2011).
[18] R. H. Liu, X. G. Luo, M. Zhang, A. F. Wang, J. J. Ying, X. F. Wang, Y. J. Yan, Z. J. Xiang, P. Cheng, G. J. Ye, Z. Y. Li, and X. H. Chen, Europhys. Lett. **94**, 27008 (2011).
[19] F. Grønvold, H. Haraldsen, and J. Vihovde, Acta Chem. Scand. **8**, 1927 (1954).
[20] D. Fruchart, P. Convert, P. Wolfers, R. Madar, J. P. Senateur, and R. Fruchart, Mater. Res. Bull. **10**, 169 (1975).
[21] H. Katsuraki and N. Achiwa, J. Phys. Soc. Jpn. **21**, 2238 (1966).
[22] C. de la Cruz, Q. Huang, J. W. Lynn, J. Li, W. Ratcliff, J. L. Zarestky, H. A. Mook, G. F. Chen, J. L. Luo, N. L. Wang, and P. C. Dai, Nature (London) **453**, 899 (2008).
[23] Q. Huang, Y. Qiu, W. Bao, M. A. Green, J. W. Lynn, Y. C. Gasparovic, T. Wu, G. Wu, and X. H. Chen, Phys. Rev. Lett. **101**, 257003 (2008).
[24] W. Bao, Y. Qiu, Q. Huang, M. A. Green, P. Zajdel, M. R. Fitzsimmons, M. Zhernenkov, M. Fang, B. Qian, E. K. Vehstedt, J. Yang, H. M. Pham, L. Spinu, and Z. Q. Mao, Phys. Rev. Lett. **102**, 247001 (2009).
[25] S. L. Li, C. de la Cruz, Q. Huang, Y. Chen, J. W. Lynn, J. P. Hu, Y. L. Huang, F. C. Hsu, K. W. Yeh, M. K. Wu, and P. C. Dai, Phys. Rev. B **79**, 054503 (2009).
[26] L. J. Zhang, D. J. Singh, and M. H. Du, Phys. Rev. B **79**, 012506 (2009).
[27] T. J. Liu, X. Ke, B. Qian, J. Hu, D. Fobes, E. K. Vehstedt, H. Pham, J. H. Yang, M. H. Fang, L. Spinu, P. Schiffer, Y. Liu, and Z. Q. Mao, Phys. Rev. B **80**, 174509 (2009).
[28] M. E. Badding, J. Li, F. J. Disalvo, W. Zhou, and P. P. Edwards, J. Solid State Chem. **100**, 313 (1992).
[29] S. X. Liu, G. L. Cai, and J. L. Huang, Acta Crystallogr. Sect. C **49**, 4 (1993).
[30] C. Pérez Vicente, M. Womes, J. C. Jumas, L. Sánchez, and J. L. Tirado, J. Phys. Chem. B **102**, 8712 (1998).
[31] J. L. Huang, Science in China Series B: Chemistry **43**, 337 (2000).
[32] J. G. Checkelsky, M. Lee, E. Morosan, R. J. Cava, and N. P. Ong, Phys. Rev. B **77**, 014433 (2008).
[33] C. G. Zeng, Y. G. Yao, Q. Niu, and H. H. Weitering, Phys. Rev. Lett. **96**, 037204 (2006).
[34] N. Nagaosa, J. Sinova, S. Onoda, A. H. MacDonald, and N. P. Ong, Rev. Mod. Phys. **82**, 1539 (2010).
[35] E. Fawcett, Rev. Mod. Phys. **60**, 209 (1988).
[36] G. Grüner, Rev. Mod. Phys. **66**, 1 (1994).
[37] G. Grüner, *Density Waves in Solids* (Addison-Wesley, Singapore, 1994).